HHS Public Access

Author manuscript

Cell Rep. Author manuscript; available in PMC 2019 September 18.

Published in final edited form as:

Cell Rep. 2019 June 11; 27(11): 3284–3294.e6. doi:10.1016/j.celrep.2019.05.048.

N-Glycolylneuraminic Acid as a Receptor for Influenza A Viruses

Frederik Broszeit[1], **Netanel Tzarum**[2], **Xueyong Zhu**[2], **Nikoloz Nemanichvili**[3], **Dirk Eggink**[4], **Tim Leenders**[1], **Zeshi Li**[1], **Lin Liu**[5], **Margreet A. Wolfert**[1,5], **Andreas Papanikolaou**[3], **Carles Martínez-Romero**[6,7], **Ivan A. Gagarinov**[1], **Wenli Yu**[2], **Adolfo García-Sastre**[6,7,8], **Tom Wennekes**[1], **Masatoshi Okamatsu**[9], **Monique H. Verheije**[3], **Ian A. Wilson**[2,10], **Geert-Jan Boons**[1,5], **Robert P. de Vries**[1,11,*]

[1]Department of Chemical Biology & Drug Discovery, Utrecht Institute for Pharmaceutical Sciences, Utrecht University, 3584 CG Utrecht, the Netherlands [2]Department of Integrative Structural and Computational Biology, The Scripps Research Institute, La Jolla, CA 92037, USA [3]Department of Pathobiology, Faculty of Veterinary Medicine, Utrecht University, 3584 CL Utrecht, the Netherlands [4]Department of Experimental Virology, Amsterdam Medical Centre, Amsterdam, the Netherlands [5]Complex Carbohydrate Research Center, University of Georgia, Athens, GA 30602, USA [6]Department of Microbiology, Icahn School of Medicine at Mount Sinai, New York, New York, USA [7]Global Health and Emerging Pathogens Institute, Icahn School of Medicine at Mount Sinai, New York, New York, USA [8]Department of Medicine, Division of Infectious Diseases, Icahn School of Medicine at Mount Sinai, New York, New York, USA [9]Laboratory of Microbiology, Department of Disease Control, Graduate School of Veterinary Medicine, Hokkaido University, Sapporo, Japan [10]Skaggs Institute for Chemical Biology, The Scripps Research Institute, La Jolla, CA 92037, USA [11]Lead Contact

SUMMARY

A species barrier for the influenza A virus is the differential expression of sialic acid, which can either be α2,3-linked for avians or α2,6-linked for human viruses. The influenza A virus hosts also express other species-specific sialic acid derivatives. One major modification at C-5 is N-glycolyl (NeuGc), instead of N-acetyl (NeuAc). N-glycolyl is mammalian specific and expressed in pigs and horses, but not in humans, ferrets, seals, or dogs. Hemagglutinin (HA) adaptation to either N-acetyl or N-glycolyl is analyzed on a sialoside microarray containing both α2,3- and α2,6-linkage modifications on biologically relevant N-glycans. Binding studies reveal that avian,

*Correspondence: r.vries@uu.nl.

AUTHOR CONTRIBUTIONS

R.P.d.V. designed the project; F.B., I.A.G., and Z.L. synthesized the microarray compounds; L.L. and M.A.W. printed the glycan arrays. F.B., L.L., M.A.W., and R.P.d.V. performed the glycan arrays analyses. N.T., X.Z., W.Y., I.A.W., and R.P.d.V performed HA expression and X-ray structure determination and analysis. T.L. and T.W. synthesized the compounds for the neuraminidase assay. D.E., M.O., C.M.-R., and A.G.-S. created the viruses and preformed the viral infection studies. M.O. provided numerous HA genes. N.N., A.P., and M.H.V. performed the tissue staining. F.B., N.T., X.Z., I.A.W., G.-J.B., and R.P.d.V. wrote the manuscript. All authors edited the paper.

DECLARATION OF INTERESTS

The authors declare no competing interests.

SUPPLEMENTAL INFORMATION

Supplemental Information can be found online at https://doi.org/10.1016/j.celrep.2019.05.048.

human, and equine HAs bind either N-glycolyl or N-acetyl. Structural data on N-glycolyl binding HA proteins of both H5 and H7 origin describe this specificity. Neuraminidases can cleave N-glycolyl efficiently, and tissue-binding studies reveal strict species specificity. The exclusive manner in which influenza A viruses differentiate between N-glycolyl and N-acetyl is indicative of selection.

Graphical Abstract

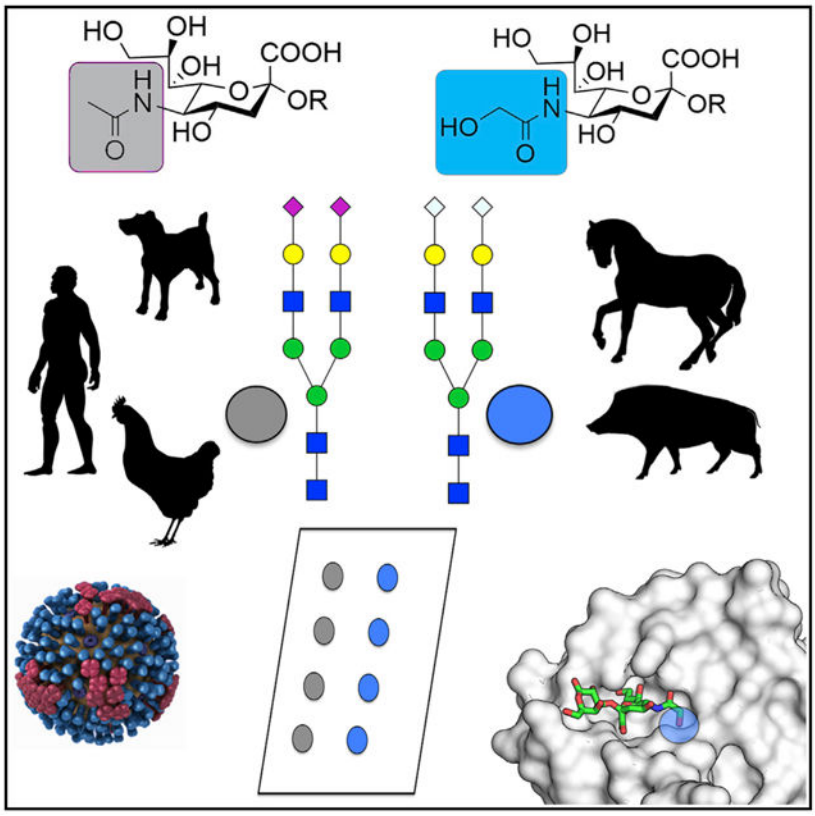

In Brief

Broszeit and colleagues demonstrate that influenza A viruses recognize either N-acetyl or N-glycolyl neuraminic acid, and they explain these specificities using X-ray structures. NeuGc-binding viruses are perfectly viable, and neuraminidases can cleave NeuGc-containing receptor structures. There is an apparent selection now for NeuAc, as no known NeuGc-binding virus currently circulates.

INTRODUCTION

The influenza A virus (IAV) is an important pathogen in animal and human health that uses sialic acids as functional receptors to gain entry into cells. The sialic acid linkage to the penultimate galactose is a species determinant for infection (de Graaf and Fouchier, 2014). Human viruses bind to α2,6-linked (human-type) sialosides present in the upper respiratory tract that enables respiratory droplet transmission (Tumpey et al., 2007). Avian viruses, on

the other hand, bind to α2,3-linked sialic acids (avian-type), which in turn are present in their respiratory and gastrointestinal tracts, enabling transmission by the oral-fecal route (Connor et al., 1994; Matrosovich et al., 2000; Paulson and de Vries, 2013).

Sialic acid is a 9-carbon monosaccharide that can contain multiple modifications that are important for a wide variety of biological events (Varki and Gagneux, 2012; Varki et al., 2015). Major modifications are N-acetyl (NeuAc) and N-glycolyl (NeuGc) structures at the C-5 position (Figure 1A); the latter is created by the hydroxylation of the N-acetyl moiety. In humans, the responsible hydroxylase contains a loss-of-function deletion that was long thought to be unique in humans, hence the term “non-human” for N-glycolyl neuraminic acid (Irie et al., 1998; Kawano et al., 1995). However, several other mammalian species have also independently lost the function of the cytidine monophosphate (CMP)-N-acetyl neuraminic acid hydroxylase (CMAH) and are, therefore, unable to synthesize N-glycolyl and only express N-acetyl. These species include dogs, ferrets, and seals (Ng et al., 2014; Peri et al., 2018; Schauer, 2016). Other mammalian species, such as horses and pigs, do express a functional CMAH enzyme and can predominantly express N-glycolyl instead of N-acetyl (Ito et al., 2000).

All IAV hemagglutinins share a highly similar receptor-binding site, consisting of absolute conserved residues Y98, W153, H183, and Y195 and conserved structural features that include the 130-, 150-, and 220-loops and the 190 helix (Skehel and Wiley, 2000). Several amino acids in these loops and helix are known to correlate with differences in receptor specificity between avian and human strains (Matrosovich et al., 2000; Rogers and Paulson, 1983; Rogers et al., 1983). However, only a few studies have analyzed N-glycolyl structures as receptors (Gambaryan et al., 2012; Higa et al., 1985; Masuda et al., 1999; Suzuki et al., 1997; Suzuki et al., 2000; Takahashi et al., 2009; Wang et al., 2012). One observation is that equine H3N8 viruses preferentially interact with N-acetyl, whereas the equine H7N7 virus binds specifically to N-glycolyl (Gambaryan et al., 2012). It has, however, been postulated that N-glycolyl might function as a decoy receptor (Takahashi et al., 2014). Finally, an H5N1 A/Vietnam/1203/04 Y161A mutant has been shown to interact only with N-glycolyl (Wang et al., 2012), and the virus replicates well in cell culture. Although these studies have provided insights into recognition of NeuGc-containing structures, they employed resialylated erythrocytes, N-glycolyl-containing gangliosides, and simple trisaccharides and have not used relevant N-linked oligosaccharide structures (Chandrasekaran et al., 2008). A notion is emerging that the complexity of oligosaccharides can modulate hemagglutinin (HA) binding (Jia et al., 2014; Peng et al., 2017; Wang et al., 2013); thus, it is important to employ biologically relevant structures. Furthermore, these studies did not report on any structural data to rationalize binding specificities.

As IAVs adapt to avian-type and human-type receptors and bind these with high selectivity, we were intrigued to investigate if adaptation to N-acetyl or N-glycolyl would result in a similar high specificity. We therefore synthesized a unique library of biologically relevant N-glycans that are found in ferret and human respiratory tissues (Jia et al., 2014; Peng et al., 2017; Walther et al., 2013) in their natural N-acetyl, as well as N-glycolyl, versions in both avian- and human-type sialic acid linkages. Using this array, we gained insights into N-acetyl and N-glycolyl specificity of several HAs of influenza A. It was found that N-glycolyl

and N-acetyl specificity is near exclusive, and using X-ray crystallography, we shed light on the receptor-binding mode. Importantly, both N-acetyl and N-glycolyl are receptors for and are cleaved by all IAV neuraminidases tested. N-glycolyl-specific HAs are unable to interact with canine tracheal epithelial cells because of the lack of CMAH in canine species. We hypothesize that N-glycolyl specificity of IAVs is selected against, based on the fact that N-glycolyl-specific viruses, such as equine H7N7 and avian H5N1 Y161A, do not currently circulate in animal hosts, and almost all tested viruses so far bind N-acetyl.

RESULTS

Synthesis of an N-glycan Library Capped with Differently Linked and Modified Sialic Acids

Glycan microarrays have become a powerful tool to analyze receptor-binding specificity of glycan-binding pathogens (Stencel-Baerenwald et al., 2014; Stevens et al., 2006a). Current arrays contain glycans modified with terminal α2,6- and α2,3-linked- N-acetyl sialic acids and include biologically relevant complex-type, biantennary N-glycans (Nycholat et al., 2012; Peng et al., 2017). To create an array that also enables N-glycolyl specificity screening, we synthesized a library of biantennary N-glycans that included both α2,6- and α2,3-linked- N-acetyl- and additionally α2,6- and α2,3-linked-N-glycolyl-derivatives. The synthesis of this sialoside array started with the extraction of a sialylglycopeptide from egg yolk (Liu et al., 2017; Seko et al., 1997). Trimming the glycopeptide resulted in starting material 1 (Figure 1A) with an asparagine at the reducing end of the N-glycan core. It was extended with additional type 2 LacNAc repeats using β3GnT2/GalT enzymes, and compounds 1, 2 and 3 each served as a starting point for sialylation (Figure 1B). Full sialylation was achieved by mammalian ST6Gal1 or bacterial PD2,6ST enzymes for α2,6-linked structures and ST3Gal4 for α2,3-linked compounds. The synthesis of the N-glycolyl derivatives was based on a one-pot procedure using a sialic acid synthetase (N. meningitidis) and CTP to generate CMP-N-glycolyl in situ. N-glycolyl was synthesized chemically according to a published procedure (Allevi et al., 2011). A comprehensive overview of the library that was used for our microarray studies is shown in Figure 1B, and the print layout is shown in Figure S1. All supporting NMR and LC-MS data of the synthetic compounds are available in Data S1. The compounds were printed on NHS-activated glass slides, and quality control of the resulting array was performed with *Erythrina cristagalli* agglutinin (ECA),*Sambuca nigra* agglutinin (SNA), and *Maackia amurensis* lectin I (MAL-I) (microarray details in Table S1 and images in Table S2). These lectins are known to be specific for terminal galactose, α2,6-linked, and α2,3-linked sialic acid, respectively. Furthermore, an antibody raised against N-glycolyl was used (Figure 1C). As expected, ECA bound only to glycans 1–3, not capped with sialic acid. SNA did not differentiate between N-glycolyl or N-acetyl and bound all α2,6-linked sialic acid-containing structures (4–6, 10, and 11), whereas MAL1 bound in an identical fashion to α2,3-linked sialic acids (7–9 and 13–15). Finally, the antibody against N-glycolyl bound all N-glycolyl-containing glycans without differentiating between the types of sialic acid linkage (10–15) (Table S3).

IAV HA Proteins Differentially Bind to N-acetyl and N-glycolyl Receptors

To analyze α2,6- and α2,3-linked N-acetyl and N-glycolyl specificity using this sialoside array, we tested binding of several influenza HA glycoproteins. These HAs were of different

origins, with some containing mutations that were reported to change receptor specificity. The H5 hemagglutinin derived from A/Vietnam/1203/04 was used as a model HA, as it selectively binds to α2,3-linked N-acetyl (7–9) (Figure 1D). We used an equine H3N8 HA to assess if this strain would bind N-glycolyl, which is predominantly expressed in the equine respiratory tract. Interestingly, this H3 HA exclusively binds to α2,3-linked N-acetyl (7–9) (Figure 1E; Table S3). Next, we wanted to reassess A/Memphis/1/71 H3N2 and its T155Y mutant, which was previously found to bind both α2,6-linked N-acetyl and N-glycolyl (Takahashi et al., 2009). For both wild-type H3N2 and the T55Y mutant, we observed binding only to α2,6-linked N-acetyl receptors (5 and 6) (Figures 1F and 1G). Next, we analyzed an equine H7 HA and demonstrated specific binding to α2,3-linked N-glycolyl receptors (14 and 15) (Figure 1H) (Gambaryan et al., 2012). Finally, we created a N-glycolyl-specific HA by introducing a Y161A mutation into A/Vietnam/1203/04 H5 (Wang et al., 2012), and this H5 Y161A mutant bound only to α2,3-linked N-glycolyl (14 and 15) (Figure 1I; Table S3). Additionally, we tested a set of wild-type HA proteins representing pandemic and seasonal human, swine, and avian H1 subtypes, a canine H3, and avian H2 and H4 subtypes. None of the proteins showed any responsiveness with N-glycolyl structures on our array and exclusively bound N-acetyl-containing glycans (Figure S2; Table S3). We conclude that the H5 Y161A mutant binds to N-glycolyl similarly to equine H7 HA and that N-acetyl and N-glycolyl specificity is exclusive.

N-glycolyl Specificity Visualized at the Atomic Level

To investigate the structural features for the switch in specificity from N-acetyl to N-glycolyl, we determined the crystal structure of the H5 Y161A mutant (Table S4). The H5 Y161A mutant crystallized as a trimer, and its overall structure is similar to the wild-type H5 HA [PDB: 3ZP0; overall Cα root-mean-square deviation (RMSD) of 0.58 Å and 0.52 Å for the HA trimer and monomer, respectively]. Nevertheless, the Y161A mutation resulted in conformational changes in the vicinity of the mutation site (residues 157–164) (Figure 2A). In addition, Y161A resulted in substantial conformational differences (residues 125–135) or disorder (residues 129–131) in the 130-loop. Y161 is part of a hydrophobic core in the vicinity of the base of the HA receptor binding site (RBS) that is formed by W127, L154, I164, and F251 (Figure 2A). Mutating the hydrophobic side chain of Y161 to an alanine resulted in a loss of hydrophobic interactions with the side chains of H130 and I164 and in significant conformational rearrangements in the hydrophobic core. Consequently, the hydrogen bond between P162 main-chain carbonyl and the side chain of H130 was lost, and amino acids 129–131 were disordered (Figures 2A and 2B).

To understand the structural basis for the receptor specificity shift to N-glycolyl, we determined the structure of the H5 Y161A mutant in complex with the 3′-GcLN (NeuGcα2–3Galβ1–4GlcNAc) at 3.3 Å resolution (Figure 2C; Table S4). Electron density was observed for two of the three monosaccharides (N-glycolyl-1 and Gal-2; Figure S3). The structure reveals that the 3′-GcLN analog binds in a cis conformation (with regards to the N-glycolyl-Gal bond), extending toward the 220-loop. Similar to the interaction of N-acetyl-1 with the base of the binding site (Figure 2D), N-glycolyl-1 forms a hydrogen bond with Y98 and also with the 130-loop, the 190-helix, and the 220-loop (Figure 2C), but there is a clear absence of hydrogen bonds to the conserved side chains of H183 and hydrophobic

interactions with the side chain of W153, which are two highly conserved interactions in N-acetyl recognition by HAs. Instead, the 1-hydroxyl of N-glycolyl-1 that distinguishes N-glycolyl from N-acetyl interacts via a hydrogen bond with the main chain of V135 and S136. Superposition of the structure of H5 Y161A HA in complex with the 3′-N-glycolyl analog to that of H5 in complex with the avian receptor analog 3′-SLN (NeuAcα2-3Galβ1–4GlcNAc) (PDB: 4BGY; Figure 2E) indicates a displacement of N-glycolyl-1 ~1.3 Å away from the base of the RBS toward the upper part of the RBS and results in a loss of interactions with H183 and W153. Superposition of N-glycolyl-1 and N-acetyl-1 (from the H5 Y161A and H5 wild-type HA structures, respectively; Figure 2F) suggests that the 3′-GcLN cannot bind to the H5 wild-type (as shown in Figure 1D) due to potential structural clashes between the N-glycolyl group of N-glycolyl-1 with the main chains of L133 and V135 from the 130-loop. Taken together, we propose that the Y161A mutation and the consequential conformational changes and disorder in the 130-loop enable binding to N-glycolyl receptors and mediate a shift toward N-glycolyl specificity.

To provide structural insights for N-glycolyl receptor specificity, we determined the crystal structure of equine H7 HA (Table S4) by molecular replacement (MR) using a homologous HA from an avian H7N3 virus (PDB: 4BSG) as the initial MR model. The Cα RMSD was 0.92 Å for the HA protomer and 0.50 Å for the receptor binding domain (residues 117–265 of HA1) between the avian and equine H7 HAs. The RBS of equine H7 HA has the same constellation of residues that are known to mediate binding specificity to α2,3-linked avian-type receptors, including Q226, G228, E190, and G225 (Xu et al., 2013) (Figure 3A), which is consistent with the finding that the equine H7 HA binds α2,3-linked N-glycolyl (Figure 1H). Because of the molecular packing in the equine H7 crystal, the HA RBS was blocked by a symmetry-related HA molecule. Thus, it was not possible to obtain an HA-receptor complex by soaking in receptor analogs. However, by superimposition of the receptor-binding domain structures of the apo H7 onto the apo H5 Y161A (Figure 3B), we found that key residues in the H5 Y161A RBS are well conserved and superim-posable in H7 HA, such as Q226, Y98, H183, S137, and G134, with E190 adopting a slightly different side-chain conformation. Although residue 135 is Glu in equine H7 HA and Val in H5 Y161A HA, the main-chain atoms of residue 135 that form important interactions with the receptor in H5 Y161A are superimposable in H5 Y161A and H7 HAs.Thus, although we did not obtain a co-crystal structure with N-glycolyl, the similarity of the essential RBS residues is suggestive of a related binding mode of both HAs to α2,3-linked N-glycolyl.

H5N1 Y161 Virus Rescue Immediately Selects for an Additional Mutation that Does Not Affect N-glycolyl Specificity

It was previously reported that an H5 virus containing the Y161A mutant had diminished plaque-forming ability (Wang et al., 2012). While rescuing this virus again, we found that a large majority of the viruses contained a second mutation, T160A. This T160A mutation results in the loss of an N-glycosylation site in the head of HA that has been implicated to be important in receptor binding and specificity for H5 HA (de Vries et al., 2014; Paulson and de Vries, 2013; Peng et al., 2018). We therefore analyzed H5 wild-type versus H5 Y161A and H5 T160A Y161A for replication efficiency in Mardin Darby canine kidney (MDCK) cells. All viruses grew efficiently in MDCK cells (Figures 4A and 4B), albeit the wild-type

grew to higher titers compared to the mutants. Next, we analyzed if equine H7N7 was able to replicate on MDCK cells with equine H3N8 and a human H3N2 virus as controls. In contrast to the N-glycolyl-specific H5 virus mutants, A/eq/49/73 H7N7 did not cause any cytopathic effect on MDCK cells and grew to very low titers, whereas the N-acetyl-specific H3 viruses replicated efficiently (Figures 4C and 4D). To analyze if the H5N1 T160A Y161A still bound to N-glycolyl sialic acids, we employed a hemagglutination assay using recombinant HAs and erythrocytes from porcine, canine, and avian origins. Porcine erythrocytes contain high levels of N-glycolyl and are not bound by the H5 wild-type but are cross linked by the single and double mutant H5 proteins (Figure 4E). As expected, the H5 wild-type protein could cross link canine and chicken erythrocytes, whereas both H5 proteins containing the Y161A mutation did not (Figure 4E). From these data, we conclude that the T160A mutation does not affect N-acetyl and N-glycolyl receptor specificity. To fully characterize the receptor specificity of the H5 Y161A T160A mutant, we analyzed this HA on our sialoside array and observed specific binding to α2,3-linked N-glycolyl (Figure 4F). We also tested if the viruses displayed strict N-acetyl or N-glycolyl specificity by glycan array analyses (Figures S4A and S4B; Table S3). Although some slight residual binding to either N-acetyl or N-acetyl can be seen, there is a clear and highly identical binding specificity compared to the recombinant HA proteins. We also observed an additional mutation in the T160A Y161A mutant virus after sequencing of the newly grown virus; R193M is located directly in the RBS, but this again did not affect N-glycolyl specificity (Figure S4B). We finally analyzed if MDCK cells are indeed N-glycolyl negative, as previously suggested (Löfling et al., 2013). Indeed, the N-glycolyl antibody efficiently stains porcine cells but did not stain MDCK and human HEK293T cells (Figure S4C). Thus, N-glycolyl-specific viruses can infect MDCK cells, although no N-glycolyl structures are present, which can possibly be explained by some residual N-acetyl binding of HA or due to neuraminidase (NA) binding.

Neuraminidases Are Able to Cleave Non-human Sialic Acids and thus Would Maintain HA-NA Balance

Because binding to N-glycolyl can, for some viruses, also support influenza infection, and because additional mutations do not affect N-glycolyl specificity, we hypothesized that the neuraminidase of A/Vietnam/1203/04 H5N1 can cleave both N-acetyl and N-glycolyl, therefore maintaining HA-NA balance. To this end, we chemically synthesized N-glycolyl-4-Methylumbelliferyl (Izumi et al., 2001; Zamora et al., 2013) (Scheme S1). We used recombinant tetrameric neuraminidases to analyze the ability of influenza virus NA proteins to cleave N-glycolyl (Bosch et al., 2010). We also analyzed a bacterial NA (Vibrio cholerae). All neuraminidases were tested in the presence and absence of CaCl2 and oseltamivir carboxylate. The H5N1 NA enzyme was able to cleave both N-acetyl and N-glycolyl, albeit the latter with lower enzymatic activity (Figure 5A) (Dai et al., 2016). Removing CaCl2 or adding oseltamivir carboxylate inhibited cleavage of sialic acid. The same specificity was observed for the NAs of H1N1 CA/04/09 and H7N9 Sh/2/13, although the latter is not dependent on CaCl2 (Smith et al., 2006) (Figures 5B and 5C). The bacterial neuraminidase derived from *Vibrio cholera* did not distinguish between N-acetyl and N-glycolyl and was not inhibited by oseltamivir carboxylate (Corfield et al., 1983) (Figure 5D). For all viral NA proteins, the cleavage rate of N-glycolyl was 2- to 4-fold lower, compared

to N-acetyl. We thus conclude that NA can cleave N-glycolyl, maintaining an HA-NA balance if HA binds N-glycolyl.

Non-human Sialic Acid Binding on Tissues

Because binding to receptors on epithelial cells of the respiratory tract is essential for infection and transmission, we analyzed binding of the HA proteins and their mutants to canine (a CMAH-negative species; Schauer, 2016) and equine (a CMAH-positive species) tracheal tissue sections. For the H5 wild-type and H3 equine proteins, we observed binding to both canine and equine trachea (Figures 6A and 6B), as both proteins are specific for α2,3-linked N-acetyl present in both tissues. On the other hand, binding of the H5 Y161A mutant and H7 equine proteins was restricted to equine tracheal tissues (Figures 6C and 6D), illustrating a strict specificity for N-glycolyl, as N-glycolyl is not synthesized in canine species. As controls, we employed an antibody to N-glycolyl that was also only able to bind equine trachea, whereas the plant lectin SNA was unable to bind either tissue, as neither contains α2,6-linked sialic acids (Figures 6E and 6F). We conclude that this strict specificity of N-glycolyl binding is a major species determinant for certain equine IAVs and mutants of other IAVs.

DISCUSSION

In this study, we analyzed the receptor specificity of HA toward N-acetyl and N-glycolyl on N-linked glycans. We demonstrate that H5 Y161A and equine H7 HAs can bind N-glycolyl and do not bind to N-acetyl, indicative of high specificity for N-glycolyl. Previous elegant studies by the research groups of Suzuki and Kawaoka (Ito et al., 2000; Masuda et al., 1999; Suzuki et al., 2000; Takahashi et al., 2009) identified that A/Memphis/1/71 T155Y virus binds to N-glycolyl, as well as N-acetyl, whereas almost all other human H3N2 viruses only recognize N-acetyl. However, when we presented H3N2 T155Y with N-glycolyl substituted onto N-glycans that are found in the human respiratory tract, instead of brain-specific gangliosides, we only observed interactions of H3N2 T155Y with N-acetyl. We also compared H5N1 wild-type and mutant viruses to the corresponding H5N1 HA proteins and observe that the viruses retain some slight residual binding to N-acetyl or N-glycolyl, respectively (Figure S4), possibly explaining the differences from our observation that H3 HA proteins have exclusive specificity for N-acetyl, whereas they can also bind N-glycolyl using whole viruses as previously shown (Takahashi et al., 2009). Another possibility could be the involvement of NA that is able to cleave N-glycolyl and, therefore, perhaps can also bind N-glycolyl and contribute as a receptor-binding site for cell entry (Hooper and Bloom, 2013; Lin et al., 2010; Zhu et al., 2012).

N-glycolyl specificity by HA abrogates binding to respiratory epithelial cells in species with a defective CMAH gene, as exemplified using canine trachea. We hypothesize that the zoonotic capabilities of equine H3N8 viruses are due to specificity to α2,3-linked N-acetyl (Collins et al., 2014; Gambaryan et al., 2012). The α2,3-linked N-acetyl is present in multiple influenza hosts, and H3N8 viruses can thus transmit with ease (Xie et al., 2016). On the other hand, equine H7N7 strictly binds to α2,3-linked N-glycolyl (Gambaryan et al., 2012), and it is tempting to conclude that this specificity led to the virus being restricted to

horses. Although equine H7N7 might be able to infect pigs and ruminants expressing N-glycolyl in the respiratory tract, experimental or observational studies for this hypothesis are lacking. On the other hand, avian H7N7 viruses that bind to α2,3-linked N-acetyl (Belser et al., 2008; Gambaryan et al., 2012; Srinivasan et al., 2013) continuously circulate in wild birds and poultry.

In conclusion, we have created a glycan array containing N-glycolyl sialic acids, and using this array, we determined the specificity of several HAs to either N-acetyl or N-glycolyl. Crystal structures of H5 Y161A and equine H7 HAs explain this specificity at the atomic level. At present, no virus circulates in nature that is known to bind N-glycolyl, indicating an apparent disadvantage for a N-glycolyl-specific virus. This can be rationalized because the natural bird reservoir does not express N-glycolyl, and the equine H7N7 virus was highly pathogenic but not maintained in horses. Indeed, the H5N1 Y161A mutant is a laboratory-derived HA; however, Y161 is conserved in H5, and it is intriguing that the Y161A mutation results in a viable virus.

STAR★METHODS

CONTACT FOR REAGENT AND RESOURCE SHARING

Further information and requests for reagents should be directed to and will be fulfilled by the Lead Contact, Robert de Vries (r.vries@uu.nl).

EXPERIMENTAL MODEL AND SUBJECT DETAILS

Erythrocytes—Erythrocytes where obtained from the Department of Clinical Sciences of Companion Animals, Department of Farm Animal Health, and the Department of Equine Sciences ll at the Faculty of Veterinary Medicine, Utrecht University, the Netherlands. All erythrocytes where obtained from adult animals that are used in the educational program of the faculty of veterinary medicine. No gender or breed differences have been observed during our studies.

Tissues—Sections of formalin-fixed, paraffin-embedded canine (*Canus lupus familiaris*) and equine (*Equus ferns caballus*) trachea were obtained from the Department of Veterinary Pathobiology, Faculty of Veterinary Medicine, Utrecht University, the Netherlands.

METHODS DETAILS

Materials and reagents—Non-commercially available enzymes were expressed according to previous literature (Karwaski et al., 2002; Moremen et al., 2018; Prudden et al., 2017). The amount of enzyme that was added to the reactions is given in units (u, enzyme) per μmol (substrate) for commercial enzymes and μg (enzyme) per μmol (substrate) for in-house expressed enzymes. One unit of the commercially available enzymes is defined as the amount of enzyme that catalyzes the conversion of 1 μmol substrate per minute using the conditions provided by the supplier. Final reactants were purified with a size exclusion Biogel (P2) from BioRad in an Econo glass column (0.7 × 30 cm / 1.5 × 30 cm / 1.5 × 50 cm) and a BioFrac fraction collector from BioRad. The carbohydrate-containing fractions were visualized using thin layer chromatography and an appropriate staining reagent (15 mL

AcOH and 3.5 mL *p*-Anisaldehyde in a mixture of 350 mL EtOH and 50 mL H_2SO_4), followed by heating.

The starting material for the enzymatic synthesis was obtained from egg yolk extraction as described by Seko et al. and further optimized by others (Liu et al., 2017; Seko et al., 1997; Sun et al., 2014; Zou et al., 2012).

General procedure for the installation of LacNAc repeating units—The acceptor and UDP-GlcNAc (3.0 eq) were dissolved in HEPES buffer (50 mM, pH 9.6, 0.1 wt% BSA) containing $MnCl_2$ (20 mM) and DTT (1 mM) to a final concentration of 5 mM. β3GnTII (10 μg per mmol acceptor) and CIAP (1 u μL^{-1}, 1 u per mmol of added nucleotide) were added to the reaction mixture and incubated at 37°C overnight with gentle shaking. The progress of the reaction was monitored by LCMS. In case of incomplete conversion after 18 h, additional β3GnTII (5 μg per mmol acceptor) was added and the reaction incubated overnight. The finished reaction was lyophilized and applied to size exclusion chromatography. The carbohydrate-containing fractions were lyophilized and dissolved in a Tris buffer (50 mM, pH 7.3, 0.1wt% BSA) containing $MnCl_2$ (20 mM). UDP-Gal (3.0 eq), CIAP (1 u μL^{-1}, 1 u per μmol of added nucleotide) and GalT (33 mu per μmol substrate) were added and the reaction mixture was incubated at 37°C overnight with gentle shaking. The progress of the reaction was monitored by LCMS. In case of incomplete conversion after 18 h, additional UDP-Gal (1.0 eq), CIAP (1 u μL^{-1}, 1 u per mmol of added nucleotide) and GalT (5 mu per μmol substrate) were added and incubated overnight. The finished reaction was lyophilized and applied to size exclusion chromatography. The carbohydrate-containing fractions were purified by high performance liquid chromatography (HPLC) giving the respective products as white powders (**2**: 1.42 mg, 66%, **3**: 1.20 mg, 71%).

Procedure for the installation of 2,6 linked NeuAc using PD2,6ST—The acceptor and CMP-Neu5Ac (1.5 eq per NeuAc) were dissolved in a Tris buffer (100 mM, pH 9, 0.1 wt% BSA) to obtain a final concentration of 5 mM. PD2,6ST (0.05 u per μmol acceptor) and CIAP (1 u μL^{-1}, 1 u per μmol of added nucleotide) were added to the reaction mixture and incubated at 37°C overnight with gentle shaking. The progress of the reaction was monitored by LCMS. In case of incomplete conversion after 18 h, additional PD2,6ST (0.05 u per μmol acceptor) was added and incubated overnight. The finished reaction was lyophilized and applied to size exclusion chromatography. The carbohydrate-containing fractions were purified by HPLC giving the product as a white powder (**4**: 0.62 mg, 56%).

General procedure for the installation of 2,6 linked NeuAc using ST6Gal1—The acceptor and CMP-Neu5Ac(1.5-2.0 eq per NeuAc) were dissolved in a sodium cacodylate buffer (100 mM, pH 7.5, 0.1 wt% BSA) to a final concentration of 1 mM.ST6Gal1 (20 μg per μmol acceptor) and CIAP (1 u μL^{-1}, 1 uper μmol of added nucleotide) were added to the reaction mixture and was incubated at 37°C overnight with gentle shaking. The progress of the reaction was monitored by LCMS. In case of incomplete conversion after 18 h, additional ST6Gal1 (5 μg per μmol acceptor) was added and incubated overnight. The finished reaction was lyophilized and applied to size exclusion chromatography. The carbohydrate-containing fractions were lyophilized and purified by HPLC giving the respective products as white powders (**5**: 0.31 mg, 51%; **6**: 0.83 mg, 71%).

General procedure for the installation of 2,6 linked NeuGc using ST6Gal1—The acceptor, NeuGc (4.0 eq) and CTP (4.0 eq) were dissolved in a $MgCl_2$ (20 mM) containing Tris buffer (100 mM, pH 8.5) to a final concentration of 2 mM. CMP-sialic acid synthetase, ST6Gal1 (20 μg per μmol acceptor) and CIAP (1 u μL^{-1}, 1 u per μmol of added nucleotide) were added to the reaction mixture and incubated at 37° C overnight with gentle shaking. The progress of the reaction was monitored by LCMS. In case of incomplete conversion after 18 h, additional ST6Gal1 (10 μg per μmol acceptor) was added and the reaction incubated overnight. The finished reaction was lyophilized and applied to size exclusion chromatography. The carbohydrate-containing fractions were lyophilized and purified by HPLC giving the respective products as white powders (**10**: 0.80 mg, 59%; **11**: 1.27 mg, 72%; **12**: 0.74 mg, 51%). (Note: **10** required extensive incubation and additional ST6Gal1.)

General procedure for the installation of 2,3 linked NeuAc using ST3Gal4—The acceptor and CMP-Neu5Ac (1.5-2.0 eq per NeuAc) were dissolved in a sodium cacodylate buffer (100 mM, pH 7.5, 0.1wt% BSA) to a final concentration of 2 mM. ST3Gal4 (20 μg per mmol acceptor) and CIAP (1 u μL^{-1},1 u per μmol of added nucleotide) were added to the reaction mixture and incubated at 37° C overnight with gentle shaking. The progress of the reaction was monitored by LCMS. In case of incomplete conversion after 18 h additional ST3Gal4 (10 μg per μmol acceptor) was added and incubated overnight. The finished reaction was lyophilized and applied to size exclusion chromatography. The carbohydrate-containing fractions were purified by HPLC giving the respective products as white powders (**7**: 0.51 mg, 65%; **8**: 0.53 mg, 58%; **9**: 0.71 mg, 60%).

General procedure for the installation of 2,3 linked NeuGc using ST3Gal4—The acceptor, NeuGc (4.0 eq) and CTP (4.0 eq) were dissolved in a $MgCl_2$ (20 mM) containing Tris buffer (100 mM, pH 8.5) to a final concentration of 2 mM. CMP-sialic acid synthetase, ST6Gal1 (20 μg per μmol acceptor) and CIAP (1 u μL^{-1}, 1 u per μmol of added nucleotide) were added to the reaction mixture and incubated at 37° C overnight with gentle shaking. The progress of the reaction was monitored by LCMS. In case of incomplete conversion after 18 h, additional ST6Gal1 (10 μg per μmol acceptor) was added and incubated overnight. The finished reaction was lyophilized and applied to size exclusion chromatography. The carbohydrate-containing fractions were purified by HPLC giving the respective products as white powders (**13**: 0.34 mg, 51%; **14**: 0.48 mg, 52%; **15**: 0.79 mg, 45%).

Synthesis of biantennary N-glycans and microarray implementation—The starting material for the enzymatic synthesis was obtained from egg yolk extraction as described by Seko et al. and further optimized by several groups (Liu et al., 2017; Seko et al., 1997; Sun et al., 2014). For this work, a recently published protocol was used, resulting in **1** as a starting material (Liu et al., 2017). Enzymatic synthesis was performed by the following general procedure: the acceptor and donor were dissolved in an appropriate buffer and, after addition of the required enzymes, incubated at 37° C overnight. Reactions were monitored by LCMS and, in case of incomplete conversion, additional enzyme and donor were added. The process was repeated until no further enzyme reaction was observed and followed by size exclusion chromatography. Purification of final compounds was

accomplished by high performance liquid chromatography (hydrophilic liquid interaction chromatography, Waters, XBridge BEH, Amide column) and yields were quantified by NMR spectroscopy.

NMR—NMR spectra were recorded at room temperature on a 600 MHz instrument from Bruker and a 400 MHz from Agilent. The chemical shift δ is given in parts per million (ppm) with reference to tetramethylsilane and the residual solvent peak [^{1}H-NMR: $\delta(D_2O)$ = 4.79 ppm]. NMR data are given as follows: ^{1}H-NMR: chemical shift (multiplicity, coupling constants, relative integral, functional group); ^{13}C data are extracted from HSQC spectra and given as follows: chemical shift. Multiplicity is defined as follows: b = broad; s = singlet; d = doublet; t = triplet; q = quartet; m = multiplet or combinations of the above. In case of superimposed peaks, the number is given before the functional group. The labeling of signals is indicated supplemental data 1 assignment was done by using corresponding 2D-NMR spectra (COSY, HSQC). The anomeric peak of Mannose-3 was hidden by the H_2O signal and assigned using the HSQC. Proton peaks that could not be assigned with the recorded spectra are indicated by “Hex.”

Due to the use of ammonium formate containing buffers during final purification, several spectra show residual formic acid (8.46 ppm) contamination. Since printing is not affected by formic acid and the yield/concentration of the products were determined by NMR spectroscopy, using n-propanol as an internal standard, the formic acid residues were not removed.

HPLC and LCMS—Analytical high-performance liquid chromatography (HPLC) was performed on a Shimadzu system (system controller: SCL10A-VP; HPLC pumps:LC10AD-VP; injector: SIL10AD-VP) using a ZIC HILIC column (ZeQuant, PEEK coated guard HPCL column, 3.5 μm particle size, 20 × 2.1 mm). The LC system was attached to a Bruker Daltonics microTOF-Q mass spectrometer. LC-conditions are indicated with each compound using the mass detector with a range of detection from 300 to 3000 Th. The reoccurring peak at 966.0 Th is an internal impurity of the instrument and not a contamination of the compounds.

For semi-preparative HPLC runs, a similar Shimadzu system (system controller: SCL10A; HPLC pumps: LC10AD) equipped with a UV detector (SPD10A-VD) and a semi-preparative XBridge HILIC column (4.6 mm (Ø) × 250 mm (l), 5 μm particle size) was used.

The solvents were purchased from Biosolve in HPLC- and LC-MS grade for preparative and analytical applications respectively. Water was deionized with a Synergy Millipore system. All solvents used for the purification of compounds was degassed by vacuum filtration prior to use. Products were detected at a wavelength of 210 nm. The following buffers were used: semi-preparative: A: 100% H_2O, 10 mM NH_4HCOO, pH 3.6; B: 10% H_2O in MeCN, 10 mM NH_4HCOO, pH 3.6; analytical: A: 100% H_2O, 30 mM NH_4HCOO, pH 3.6; B: 100% MeCN.

High resolution masses were obtained by using an Agilent 6560 Ion Mobility Q-TOF LC-MS system.

Microarray printing—All compounds were printed on NHS-ester activated glass slides (NEXTERION ® Slide H, Schott Inc.) using a Scienion sciFLEXARRAYER S3 non-contact microarray equipped with a Scienion PDC80 nozzle (Scienion Inc.). Individual compounds were dissolved in sodium phosphate buffer (250 mM, pH 8.5) at a concentration of 100μM and were printed in replicates of 6 with spot volume ~400pL, at 20°C and 50% humidity. Each slide has 24 subarrays in a 3×8 layout. After printing, slides were incubated in a humidity chamber for 8 h and then blocked for 1 h with a 50mM ethanolamine in Tris buffer (pH 9.0, 100 mM) at 50°C. Blocked slides were rinsed with DI water, spun dry, and kept in a desiccator at room temperature for future use.

Scanning: After staining, the slides were scanned using a GenePix 4000B microarray scanner (Molecular Devices) at the appreciate excitation wavelength with a resolution of 5μM. Various gains and PMT values were employed in the scanning to ensure that all signals were within the linear range of the scanner's detector and no saturation of the signals.

Data processing: The data were analyzed with our home written Excel macro. The highest and the lowest value of the total fluorescence intensity of the six replicates spots were removed to provide the mean value and standard deviation (n = 4).

Quality control:The printing was validated by several lectins including *Erythrina cristagalli* agglutinin (ECA, specific for terminal Gal), *Sambuca nigra* agglutinin (SNA, specific for terminal α2,6-NeuAc/NeuGc), *Maackia amurensis* lectin I (MAL-I, specific for α2,3-NeuAc/NeuGc) and an anti-NeuGc antibody. The biotinylated lectins were visualized with Streptavidin-AlexaFluor635. After staining, the slides were scanned at the appropriate excitation wavelength and images were analyzed.

Expression and purification of HA for binding studies—HA encoding cDNAs (Genscript, USA), were cloned into the pCD5 expression as described previously (de Vries et al., 2010). The pCD5 expression vector was adapted so that the HA-encoding cDNAs are cloned in frame with DNA sequences coding for a signal sequence, a GCN4 trimerization motif (RMKQIEDKIEEIESKQKKIENEIARIKK), a super folder GFP (Sliepen et al., 2015), and the Strep-tag II (WSHPQFEKGGGSGGGSWSHPQFEK); IBA, Germany).

HA proteins were expressed in HEK293S GnTI(−) cells and purified from the cell culture supernatants as described previously (de Vries et al., 2010). pCD5 expression vectors were transfected into HEK293S GnTI(−) cells using polyethyleneimine I (PEI). At 6 h post transfection, the transfection mixture was replaced by 293 SFM II expression medium (GIBCO), supplemented with sodium bicarbonate (3.7 g/L), glucose (2.0 g/L), Primatone RL-UF (3.0 g/L), glutaMAX (GIBCO), valproic acid (0,4 g/L) and DMSO (1,5%). Tissue culture supernatants were harvested 5–6 days post transfection. HA proteins were purified using Strep-Tactin Sepharose beads according to the manufacturer's instructions (IBA, Germany).

Glycan microarray binding of HA—Recombinant HA were precomplexed with mouse anti-streptag-Alexa647 and goat-anti mouse-Alexa647 antibodies in a 4:2:1 molar ratio in 50 μL PBS-T. This mixture was incubated on ice for 15 min and subsequently incubated on the array surface in a humidified chamber for 90 min. Slides were subsequently washed by successive rinses with PBS-T, PBS, and deionized H_2O. Washed arrays were dried by centrifugation and immediately scanned and processed identical to the plant lectins described above.

Expression and purification of the H5 Y161A HA mutant for crystallization—The cDNA of A/Vietnam/1203/04 [GISAID accession number: EF541403] was cloned into a pFastBac vector and the Y161A mutation was generated by site-directed mutagenesis. The H5 Y161A HA was expressed in Hi5 insect cells with an N-terminal gp67 signal peptide, C-terminal thrombin cleavage site, foldon trimerization sequence, and His_6-tag and expressed as described previously (Stevens et al., 2006b). The expressed HA0 was purified via His-tag affinity purification, dialyzed against 20 mM Tris-HCl pH 8.0, 100 mM NaCl, and then cleaved by trypsin (New England Biolabs, Ipswich, MA) to produce uniformly cleaved (HA1/HA2) and to remove the trimerization domain and His_6-tag. The digested protein was purified further by Superdex-200 gel filtration chromatography (Pharmacia). The HA protein eluted as a trimer and was concentrated to 5 mg/mL.

Crystallization and structural determination of the H5 Y161A HA—Crystals of the Y161A mutant were obtained using the vapor diffusion sitting drop method at 4°C against a reservoir solution containing 20% (w/v) PEG 3350, 0.1 M Na-Acetate, pH 7.0. The complex of HA proteins with receptor analog 3′-GcLN was obtained by soaking HA crystals in the reservoir solution that contained the glycan ligand to a final concentration of 5 mM. Prior to data collection, the crystals were cryoprotected using 10% ethylene glycol and flash cooled in liquid nitrogen. Diffraction data were collected at the Advanced Photon Source (APS) and at the Stanford Synchrotron Radiation Lightsource (SSRL) (Table S4). Data were integrated and scaled using HKL2000 (Otwinowski and Minor, 1997). The initial H5 Y161A apo structure was solved by molecular replacement method using Phaser (McCoy et al., 2005) with H5 wild-type HA structure (PDB: 2FK0) as the search model. The refined H5 Y161A HA apo structure was then used as the starting model for structure determination of the H5 HA-3′-NeuGc complex structures. Structure refinement was carried out in Phenix (Adams et al., 2002) and model with COOT (Emsley and Cowtan, 2004). Final refinement statistics are summarized in Table S4.

Expression and purification of the equine H7 HA for crystallization—The cDNA of A/equine/NY/49/73/H7N7 was cloned into a pFastbac vector, and the H7 HA expressed in Hi5 insect cells with an N-terminal gp67 signal peptide, C-terminal thrombin cleavage site, foldon trimerization sequence, and His_6-tag and expressed as described previously (Stevens et al., 2006b). The expressed HA0 was purified by Ni-NTA affinity purification, dialyzed against 20 mM Tris-HCl pH 8.0, 100 mM NaCl, and then cleaved by thrombin (MilliporeSigma, Burlington, MA) to remove the trimerization domain and His_6-tag. The H7 HA protein was further purified by Superdex-200 gel filtration chromatography (Pharmacia). The purified HA protein eluted as a trimer and was concentrated to 6 mg/ml.

Crystallization and structural determination of the equine H7 HA—Crystals of equine H7 HA were obtained using the vapor diffusion sitting drop method at 20°C against a reservoir solution containing 0.1 M HEPES, pH 6.5, 2.4 M ammonium sulfate. Prior to data collection, the crystals were cryoprotected with 25% ethylene glycol and flash cooled in liquid nitrogen. Diffraction data were collected at the Stanford Synchrotron Radiation Lightsource (SSRL) (Table S4). Data were integrated and scaled using HKL2000 (Otwinowski and Minor, 1997). The H7 apo structure was solved by molecular replacement method using Phaser (McCoy et al., 2005) with an avian H7 wild-type HA structure (PDB: 4BSG) as a search model. Structure refinement was carried out in REFMAC5 (Murshudov et al., 2011) and modeled with COOT (Emsley and Cowtan, 2004). Final refinement statistics are summarized in Table S4.

Virus infectivity and hemagglutination—The viruses were generated as described previously (Wang et al., 2012). Briefly, a coculture of MDCK and 293T cells was transfected with four expression plasmids coding for the PB1, PB2, and PA proteins and nucleoprotein (NP) and with eight pPolI plasmids, each containing one of the HA virus viral RNA (vRNA) segments, including the wild-type HA segment, or their corresponding mutant HA genes. All internal genes are PR8 HALo. A total of 0.5 to 1 μg of each plasmid was transfected using Lipofectamine 2000 (Invitrogen, Carlsbad, CA). At 12 h post transfection, the medium was replaced by DMEM containing 0.3% bovine serum albumin, 10 mM HEPES, and 1 μg of tosylsulfonyl phenylalanyl chloromethyl ketone (TPCK)-treated trypsin/mL. At 3 days post transfection, virus within the cell supernatants was plaque purified by titration on MDCK cells. All the segments of the recovered mutant viruses were analyzed by reverse transcription-PCR (RT-PCR) and confirmed by sequencing.

MDCK cells were infected at a multiplicity of infection (MOI) of 0.01 with recombinant influenza A viruses expressing either HA Y161A, HA T160A Y161A, or parental HA and equine and human influenza A viruses. At 0, 12, 24, 36, 48, and 60 h post infection, cell supernatants were harvested and titrated on fresh MDCK cells.

Hemagglutination assays were performed with 0.5% erythrocytes using HA pre-complexed as described previously (de Vries et al., 2010) at a starting concentration of 10 μg/mL.

Neuraminidase specificity and activity—2′-(4-Methylumbelliferyl)-α-D-N-glycolylneuraminic acid was synthesized previously (Izumi et al., 2001; Zamora et al., 2013) (Scheme S1). The synthesis used in this paper is partially based on the method used by Zamora et al. by protecting the C5 position with a Boc group to selectively deprotect and introduce the glycolyl group. Chlorination of the anomeric position with *in situ* HCl gas and subsequent glycosylation with sodium-4-methylumbelliferone gave sufficient yields to perform the experiments.

NA solution-based enzymatic activities were measured in PBS at pH 6.15 supplemented with 10 mM $CaCl_2$, using the fluorescent substrate 2′-(4-methylumbelliferyl)-α-D-N-acetylneuraminic acid (4-MU-NANA; Sigma [Potier et al., 1979; Xu et al., 2012]) and 2′-(4-methylumbelliferyl)-α-D-N-glycolylneuraminic acid (4-MU-NGNA). The reaction was conducted at room temperature in a total volume of 80 μL. After the reaction mixture was

incubated for 1 h, the reaction was stopped by addition of 80 μL 1 M Na_2CO_3. The reactions were measured at excitation and emission wavelengths of 365 nm and 450 nm, respectively. The reactions were all performed in triplicate.

Tissue staining—Tissue sections were rehydrated in series of alcohol from 100%, 96% to 70% and lastly in distilled water. Endogenous peroxidase activity was blocked with 1% hydrogen peroxide for 30 min. Tissues slides were boiled in citrate buffer pH 6.0 for 10 min at 900 kW in a microwave for antigen retrieval and washed in PBS-T three times. Tissues were subsequently incubated with 3% BSA in PBS-T overnight at 4°C. The next day, the purified, soluble trimeric HA was pre-complexed with mouse anti-strep-tag-HRP antibodies (IBA) and goat anti-mouse IgG HRP antibodies (Life Biosciences) in a ratio of 4:2:1 in PBS-T with 3% BSA and incubated on ice for 15 min. After draining the slide, the pre-complexed HA was applied onto the tissue and incubated for 90 min. Sections were then washed in PBS-T, incubated with 3-amino-9-ethyl-carbazole (AEC; Sigma-Aldrich) for 15 min, counterstained with hematoxylin and mounted with Aquatex (Merck). Images were taken using a charge-coupled device (CCD) camera and an Olympus BX41 microscope linked to CellB imaging software (Soft Imaging Solutions GmbH, Münster, Germany).

QUANTIFICATION AND STATISTICAL ANALYSIS

Glycan microarray—Data are plotted from fluorescent intensity, analyzed using GenePix Pro 7 software, from the images, the highest and lowest value where removed from 6 replicates, total intensities are plotted as means ± SD. The data were further processed with Microsoft Excel and plotted with GraphPad Prism 7. The data are representative of three independent assays using independently made protein preparations.

Infectivity of viruses—A representative of three independent assays is shown and plotted as means ± SD. The data were processed with Microsoft Excel and plotted with GraphPad Prism 7.

Hemagglutination—The data are representative of three independent assays performed in triplicate, using independently made protein preparations and plotted as means ± SD. The data were processed with Microsoft Excel and plotted with GraphPad Prism 7.

Neuraminidase activity—The data are representative of three independent assays performed in triplicate, using independently made protein preparations and plotted as means ± SD. The data were processed with Microsoft Excel and plotted with GraphPad Prism 7.

Tissue binding—The data are representative of three independent assays with independent protein preparations. Tissues from different paraffin blocks where used (n = 3).

DATA AND SOFTWARE AVAILABILITY

Tabulated microarray data are provided in Table S3. Atomic coordinates and structure factors have been deposited in the Protein Data Bank (PDB) under accession codes 6E7G for H5N1 HA in apo form and 6E7H in complex with 3′-GcLN and 6N5A for H7N7 HA. The A/equine/NY/49/73 HA sequence is deposited in the NCBI database (LC414434).

ADDITIONAL RESOURCES

All NMR and LC-MS data on the synthesized compounds can be found online in the Data S1 file.

Supplementary Material

Refer to Web version on PubMed Central for supplementary material.

ACKNOWLEDGMENTS

R.P.d.V. is a recipient of a VENI grant from the Netherlands Organization for Scientific Research (NWO), an ERC Starting Grant from the European Commission (802780), and a Beijerinck Premium of the Royal Dutch Academy of Sciences. Synthesis and microarray analysis were funded by a grant from NWO (TOPPUNT 718.015.003 to G.-J.B. and VIDI 723.014.005 to T.W.) and Utrecht University. This work was funded in part by NIH grant R56 AI127371 (to I.A.W). M.H.V is a recipient of a MEERVOUD grant from the NWO. This work was also in part funded by CRIP (Center for Research on Influenza Pathogenesis) and NIAID-funded Center of Excellence for Influenza Research and Surveillance (CEIRS; contract #HHSN272201400008C) to A.G.-S. X-ray data sets were collected at the APS beamline 23ID-B (GM/CA CAT) and SSRL beamline 12-2. The use of the APS was supported by the U.S. Department of Energy (DOE), Basic Energy Sciences, Office of Science, under contract DE-AC02-06CH11357. The SSRL Structural Molecular Biology Program was supported by the DOE Office of Biological and Environmental Research and by the NIH NIGMS (including P41GM103393) and the National Center for Research Resources (P41RR001209). We thank Dr. James Paulson (The Scripps Research Institute, La Jolla, USA) for fruitful discussions. Furthermore, we thank Dr. Roland Corbee and Inge van Duiven (Department of Companion Animals), Francisca Velkers (Department of Farm Animal Health, Faculty of Veterinary Medicine, Utrecht University, the Netherlands), and the animal caretakers of Department of Equine Sciences (Faculty of Veterinary Medicine, Utrecht University, the Netherlands) for supplying erythrocytes.

REFERENCES

Adams PD, Grosse-Kunstleve RW, Hung LW, Ioerger TR, McCoy AJ, Moriarty NW, Read RJ, Sacchettini JC, Sauter NK, and Terwilliger TC (2002). PHENIX: building new software for automated crystallographic structure determination. Acta Crystallogr. D Biol. Crystallogr. 58, 1948–1954. [PubMed: 12393927]

Allevi P, Anastasia M, Costa ML, and Rota P (2011). Two procedures for the syntheses of labeled sialic acids and their 1,7-lactones. Tetrahedron Asymmetry 22, 338–344.

Belser JA, Blixt O, Chen LM, Pappas C, Maines TR, Van Hoeven N, Donis R, Busch J, McBride R, Paulson JC, et al. (2008). Contemporary North American influenza H7 viruses possess human receptor specificity: Implications for virus transmissibility. Proc. Natl. Acad. Sci. USA 105,7558–7563. [PubMed: 18508975]

Bosch BJ, Bodewes R, de Vries RP, Kreijtz JH, Bartelink W, van Amerongen G, Rimmelzwaan GF, de Haan CA, Osterhaus AD, and Rottier PJ (2010). Recombinant soluble, multimeric HA and NA exhibit distinctive types of protection against pandemic swine-origin 2009 A(H1N1) influenza virus infection in ferrets. J. Virol. 84, 10366–10374. [PubMed: 20686020]

Chandrasekaran A, Srinivasan A, Raman R, Viswanathan K, Raguram S, Tumpey TM, Sasisekharan V, and Sasisekharan R (2008). Glycan topology determines human adaptation of avian H5N1 virus hemagglutinin. Nat. Biotechnol. 26, 107–113. [PubMed: 18176555]

Collins PJ, Vachieri SG, Haire LF, Ogrodowicz RW, Martin SR, Walker PA, Xiong X, Gamblin SJ, and Skehel JJ (2014). Recent evolution of equine influenza and the origin of canine influenza. Proc. Natl. Acad. Sci. USA 111, 11175–11180. [PubMed: 25024224]

Connor RJ, Kawaoka Y, Webster RG, and Paulson JC (1994). Receptor specificity in human, avian, and equine H2 and H3 influenza virus isolates. Virology 205, 17–23. [PubMed: 7975212]

Corfield AP, Higa H, Paulson JC, and Schauer R (1983). The specificity of viral and bacterial sialidases for α(2-3)- and α(2-6)-linked sialic acids in glycoproteins. Biochim. Biophys. Acta 744, 121–126. [PubMed: 6301560]

Dai M, Guo H, Dortmans JC, Dekkers J, Nordholm J, Daniels R, van Kuppeveld FJ, de Vries E, and de Haan CA (2016). Identification of residues that affect oligomerization and/or enzymatic activity of influenza virus H5N1 neuraminidase proteins. J. Virol. 90, 9457–9470. [PubMed: 27512075]

de Graaf M, and Fouchier RA (2014). Role of receptor binding specificity in influenza A virus transmission and pathogenesis. EMBO J. 33, 823–841. [PubMed: 24668228]

de Vries RP, de Vries E, Bosch BJ, de Groot RJ, Rottier PJ, and de Haan CA (2010). The influenza A virus hemagglutinin glycosylation state affects receptor-binding specificity. Virology 403, 17–25. [PubMed: 20441997]

de Vries RP, de Vries E, Moore KS, Rigter A, Rottier PJ, and de Haan CA (2011). Only two residues are responsible for the dramatic difference in receptor binding between swine and new pandemic H1 hemagglutinin. J. Biol. Chem. 286, 5868–5875. [PubMed: 21173148]

de Vries RP, Zhu X, McBride R, Rigter A, Hanson A, Zhong G, Hatta M, Xu R, Yu W, Kawaoka Y, et al. (2014). Hemagglutinin receptor specificity and structural analyses of respiratory droplet-transmissible H5N1 viruses. J. Virol. 88, 768–773. [PubMed: 24173215]

Emsley P, and Cowtan K (2004). Coot: model-building tools for molecular graphics. Acta Crystallogr. D Biol. Crystallogr 60, 2126–2132. [PubMed: 15572765]

Gambaryan AS, Matrosovich TY, Philipp J, Munster VJ, Fouchier RA, Cattoli G, Capua I, Krauss SL, Webster RG, Banks J, et al. (2012). Receptor-binding profiles of H7 subtype influenza viruses in different host species. J. Virol. 86, 4370–4379. [PubMed: 22345462]

Higa HH, Rogers GN, and Paulson JC (1985). Influenzavirus hemagglutinins differentiate between receptor determinants bearing N-acetyl-, N-glycollyl-, and N,O-diacetylneuraminic acids. Virology 144, 279–282. [PubMed: 4060591]

Hooper KA, and Bloom JD (2013). A mutant influenza virus that uses an N1 neuraminidase as the receptor-binding protein. J. Virol. 87, 12531–12540. [PubMed: 24027333]

Irie A, Koyama S, Kozutsumi Y, Kawasaki T, and Suzuki A (1998). The molecular basis for the absence of N-glycolylneuraminic acid in humans. J. Biol. Chem. 273, 15866–15871. [PubMed: 9624188]

Ito T, Suzuki Y, Suzuki T, Takada A, Horimoto T, Wells K, Kida H, Otsuki K, Kiso M, Ishida H, and Kawaoka Y (2000). Recognition of N-glycolylneuraminic acid linked to galactose by the α2,3 linkage is associated with intestinal replication of influenza A virus in ducks. J. Virol. 74, 9300–9305. [PubMed: 10982377]

Izumi M, Shen GJ, Wacowich-Sgarbi S, Nakatani T, Plettenburg O, and Wong CH (2001). Microbial glycosyltransferases for carbohydrate synthesis: α-2,3-sialyltransferase from *Neisseria gonorrheae*. J. Am. Chem. Soc. 123, 10909–10918. [PubMed: 11686694]

Jia N, Barclay WS, Roberts K, Yen HL, Chan RW, Lam AK, Air G, Peiris JS, Dell A, Nicholls JM, and Haslam SM (2014). Glycomic characterization of respiratory tract tissues of ferrets: implications for its use in influenza virus infection studies. J. Biol. Chem. 289, 28489–28504. [PubMed: 25135641]

Karwaski MF, Wakarchuk WW, and Gilbert M (2002). High-level expression of recombinant Neisseria CMP-sialic acid synthetase in Escherichia coli. Protein Expr. Purif. 25, 237–240. [PubMed: 12135555]

Kawano T, Koyama S, Takematsu H, Kozutsumi Y, Kawasaki H, Kawashima S, Kawasaki T, and Suzuki A (1995). Molecular cloning of cytidine monophospho-N-acetylneuraminic acid hydroxylase. Regulation of species and tissue-specific expression of N-glycolylneuraminic acid. J. Biol. Chem. 270, 16458–16463. [PubMed: 7608218]

Lin YP, Gregory V, Collins P, Kloess J, Wharton S, Cattle N, Lackenby A, Daniels R, and Hay A (2010). Neuraminidase receptor binding variants of human influenza A(H3N2) viruses resulting from substitution of aspartic acid 151 in the catalytic site: a role in virus attachment? J. Virol. 84, 6769–6781. [PubMed: 20410266]

Liu L, Prudden AR, Bosman GP, and Boons GJ (2017). Improved isolation and characterization procedure of sialylglycopeptide from egg yolk powder. Carbohydr. Res. 452, 122–128. [PubMed: 29096185]

Löfling J, Lyi SM, Parrish CR, and Varki A (2013). Canine and feline parvoviruses preferentially recognize the non-human cell surface sialic acid N-glycolylneuraminic acid. Virology 440, 89–96. [PubMed: 23497940]

Masuda H, Suzuki T, Sugiyama Y, Horiike G, Murakami K, Miyamoto D, Jwa Hidari KI, Ito T, Kida H, Kiso M, et al. (1999). Substitution of amino acid residue in influenza A virus hemagglutinin affects recognition of sialyl-oligosaccharides containing N-glycolylneuraminic acid. FEBS Lett. 464, 71–74. [PubMed: 10611486]

Matrosovich M, Tuzikov A, Bovin N, Gambaryan A, Klimov A, Castrucci MR, Donatelli I, and Kawaoka Y (2000). Early alterations of the receptorbinding properties of H1, H2, and H3 avian influenzavirus hemagglutinins after their introduction into mammals. J. Virol. 74, 8502–8512. [PubMed: 10954551]

McCoy AJ, Grosse-Kunstleve RW, Storoni LC, and Read RJ (2005). Likelihood-enhanced fast translation functions. Acta Crystallogr. D Biol. Crystallogr. 61, 458–464. [PubMed: 15805601]

Moremen KW, Ramiah A, Stuart M, Steel J, Meng L, Forouhar F, Moniz HA, Gahlay G, Gao Z, Chapla D, et al. (2018). Expression system for structural and functional studies of human glycosylation enzymes. Nat. Chem. Biol. 14, 156–162. [PubMed: 29251719]

Motoshima M, Okamatsu M, Asakura S, Kuribayashi S, Sengee S, Batchuluun D, Ito M, Maeda Y, Eto M, Sakoda Y, et al. (2011). Antigenic and genetic analysis of H3N8 influenza viruses isolated from horses in Japan and Mongolia, and imported from Canada and Belgium during 2007-2010. Arch. Virol. 156, 1379–1385. [PubMed: 21505822]

Murshudov GN, Skubák P, Lebedev AA, Pannu NS, Steiner RA, Nicholls RA, Winn MD, Long F, and Vagin AA (2011). REFMAC5 for the refinement of macromolecular crystal structures. Acta Crystallogr. D Biol. Crystallogr. 67, 355–367. [PubMed: 21460454]

Nemanichvili N, Tomris I, Turner HL, McBride R, Grant OC, van der Woude R, Aldosari MH, Pieters RJ, Woods RJ, Paulson JC, et al. (2019). Fluorescent trimeric hemagglutinins reveal multivalent receptor binding properties. J. Mol. Biol. 431, 842–856. [PubMed: 30597163]

Ng PS, Böhm R, Hartley-Tassell LE, Steen JA, Wang H, Lukowski SW, Hawthorne PL, Trezise AE, Coloe PJ, Grimmond SM, et al. (2014). Ferrets exclusively synthesize Neu5Ac and express naturally humanized influenza A virus receptors. Nat. Commun. 5, 5750. [PubMed: 25517696]

Nycholat CM, McBride R, Ekiert DC, Xu R, Rangarajan J, Peng W, Razi N, Gilbert M, Wakarchuk W, Wilson IA, and Paulson JC (2012). Recognition of sialylated poly-N-acetyllactosamine chains on N-and O-linked glycans by human and avian influenza A virus hemagglutinins. Angew. Chem. Int. Ed. Engl. 51,4860–4863. [PubMed: 22505324]

Otwinowski Z, and Minor W (1997). Processing of X-ray diffraction data collected in oscillation mode. Methods Enzymol. 276, 307–326.

Paulson JC, and de Vries RP (2013). H5N1 receptor specificity as a factor in pandemic risk. Virus Res. 178, 99–113. [PubMed: 23619279]

Peng W, de Vries RP, Grant OC, Thompson AJ, McBride R, Tsogtbaatar B, Lee PS, Razi N, Wilson IA, Woods RJ, and Paulson JC (2017). Recent H3N2 viruses have evolved specificity for extended, branched human-type receptors, conferring potential for increased avidity. Cell Host Microbe 21, 23–34. [PubMed: 28017661]

Peng W, Bouwman KM, McBride R, Grant OC, Woods RJ, Verheije MH, Paulson JC, and de Vries RP (2018). Enhanced human-type receptor binding by ferret-transmissible H5N1 with a K193T mutation. J. Virol. 92, e02016–e02017. [PubMed: 29491160]

Peri S, Kulkarni A, Feyertag F, Berninsone PM, and Alvarez-Ponce D (2018). Phylogenetic distribution of CMP-Neu5Ac hydroxylase (CMAH), the enzyme synthetizing the proinflammatory human xenoantigen Neu5Gc. Genome Biol. Evol. 10, 207–219. [PubMed: 29206915]

Potier M, Mameli L, Bélisle M, Dallaire L, and Melancon SB (1979). Fluorometric assay of neuraminidase with a sodium (4-methylumbelliferyl-α-D-N-acetylneuraminate) substrate. Anal. Biochem. 94, 287–296. [PubMed: 464297]

Prudden AR, Liu L, Capicciotti CJ, Wolfert MA, Wang S, Gao Z, Meng L, Moremen KW, and Boons GJ (2017). Synthesis of asymmetrical multiantennary human milk oligosaccharides. Proc. Natl. Acad. Sci. USA 114, 6954–6959. [PubMed: 28630345]

Rogers GN, and Paulson JC (1983). Receptor determinants of human and animal influenza virus isolates: differences in receptor specificity of the H3 hemagglutinin based on species of origin. Virology 127, 361–373. [PubMed: 6868370]

Rogers GN, Paulson JC, Daniels RS, Skehel JJ, Wilson IA, and Wiley DC (1983). Single amino acid substitutions in influenza haemagglutinin change receptor binding specificity. Nature 304, 76–78. [PubMed: 6191220]

Schauer R (2016). Sialic acids as link to Japanese scientists. Proc. Jpn. Acad., Ser. B, Phys. Biol. Sci 92, 109–120.

Seko A, Koketsu M, Nishizono M, Enoki Y, Ibrahim HR, Juneja LR, Kim M, and Yamamoto T (1997). Occurence of a sialylglycopeptide and free sialylglycans in hen's egg yolk. Biochim. Biophys. Acta 1335, 23–32. [PubMed: 9133639]

Skehel JJ, and Wiley DC (2000). Receptor binding and membrane fusion in virus entry: the influenza hemagglutinin. Annu. Rev. Biochem. 69, 531–569. [PubMed: 10966468]

Sliepen K, van Montfort T, Ozorowski G, Pritchard LK, Crispin M, Ward AB, and Sanders RW (2015). Engineering and characterization of a fluorescent native-like HIV-1 envelope glycoprotein trimer. Biomolecules 5, 2919–2934. [PubMed: 26512709]

Smith BJ, Huyton T, Joosten RP, McKimm-Breschkin JL, Zhang JG, Luo CS, Lou MZ, Labrou NE, and Garrett TP (2006). Structure of a calcium-deficient form of influenza virus neuraminidase: implications for substrate binding. Acta Crystallogr. D Biol. Crystallogr. 62, 947–952. [PubMed: 16929094]

Srinivasan K, Raman R, Jayaraman A, Viswanathan K, and Sasisekharan R (2013). Quantitative description of glycan-receptor binding of influenza A virus H7 hemagglutinin. PLoS ONE 8, e49597. [PubMed: 23437033]

Stencel-Baerenwald JE, Reiss K, Reiter DM, Stehle T, and Dermody TS (2014). The sweet spot: defining virus-sialic acid interactions. Nat. Rev. Microbiol. 12, 739–749. [PubMed: 25263223]

Stevens J, Blixt O, Glaser L, Taubenberger JK, Palese P, Paulson JC, and Wilson IA (2006a). Glycan microarray analysis of the hemagglutinins from modern and pandemic influenza viruses reveals different receptor specificities. J. Mol. Biol. 355, 1143–1155. [PubMed: 16343533]

Stevens J, Blixt O, Tumpey TM, Taubenberger JK, Paulson JC, and Wilson IA (2006b). Structure and receptor specificity of the hemagglutinin from an H5N1 influenza virus. Science 312, 404–410. [PubMed: 16543414]

Sun B, Bao W, Tian X, Li M, Liu H, Dong J, and Huang W (2014). A simplified procedure for gram-scale production of sialylglycopeptide (SGP) from egg yolks and subsequent semi-synthesis of $Man_3GlcNAc$ oxazoline. Carbohydr. Res. 396, 62–69. [PubMed: 25124522]

Suzuki T, Horiike G, Yamazaki Y, Kawabe K, Masuda H, Miyamoto D, Matsuda M, Nishimura SI, Yamagata T, Ito T, et al. (1997). Swine influenza virus strains recognize sialylsugar chains containing the molecular species of sialic acid predominantly present in the swine tracheal epithelium. FEBS Lett. 404, 192–196. [PubMed: 9119062]

Suzuki Y, Ito T, Suzuki T, Holland RE Jr., Chambers TM, Kiso M, Ishida H, and Kawaoka Y (2000). Sialic acid species as a determinant of the host range of influenza A viruses. J. Virol. 74, 11825–11831. [PubMed: 11090182]

Takahashi T, Hashimoto A, Maruyama M, Ishida H, Kiso M, Kawaoka Y, Suzuki Y, and Suzuki T (2009). Identification of amino acid residues of influenza A virus H3 HA contributing to the recognition of molecular species of sialic acid. FEBS Lett. 583, 3171–3174. [PubMed: 19720062]

Takahashi T, Takano M, Kurebayashi Y, Masuda M, Kawagishi S, Takaguchi M, Yamanaka T, Minami A, Otsubo T, Ikeda K, and Suzuki T (2014). N-glycolylneuraminic acid on human epithelial cells prevents entry of influenza A viruses that possess N-glycolylneuraminic acid binding ability. J. Virol. 88, 8445–8456. [PubMed: 24829344]

Tumpey TM, Maines TR, Van Hoeven N, Glaser L, Solórzano A, Pappas C, Cox NJ, Swayne DE, Palese P, Katz JM, and García-Sastre A (2007). A two-amino acid change in the hemagglutinin of the 1918 influenza virus abolishes transmission. Science 315, 655–659. [PubMed: 17272724]

Varki A, and Gagneux P (2012). Multifarious roles of sialic acids in immunity. Ann. N Y Acad. Sci. 1253, 16–36. [PubMed: 22524423]

Varki A, Schnaar RL, and Schauer R (2015). Sialic acids and other nonulosonic acids In Essentials of Glycobiology, Varki A, Cummings RD, Esko JD, Stanley P, Hart GW, Aebi M, Darvill AG, Kinoshita T, Packer NH, and Prestegard JH, et al., eds. (Cold Spring Harbor Laboratory Press), pp. 179–195.

Walther T, Karamanska R, Chan RW, Chan MC, Jia N, Air G, Hopton C, Wong MP, Dell A, Malik Peiris JS, et al. (2013). Glycomic analysis of human respiratory tract tissues and correlation with influenza virus infection. PLoS Pathog. 9,e1003223. [PubMed: 23516363]

Wang M, Tscherne DM, McCullough C, Caffrey M, García-Sastre A, and Rong L (2012). Residue Y161 of influenza virus hemagglutinin is involved in viral recognition of sialylated complexes from different hosts. J. Virol. 86, 4455–4462. [PubMed: 22301136]

Wang Z, Chinoy ZS, Ambre SG, Peng W, McBride R, de Vries RP, Glushka J, Paulson JC, and Boons GJ (2013). A general strategy for the chemoenzymatic synthesis of asymmetrically branched N-glycans. Science 341, 379–383. [PubMed: 23888036]

Xie T, Anderson BD, Daramragchaa U, Chuluunbaatar M, and Gray GC (2016). A review of evidence that equine influenza viruses are zoonotic. Pathogens 5, E50. [PubMed: 27420100]

Xu R, Zhu X, McBride R, Nycholat CM, Yu W, Paulson JC, and Wilson A (2012). Functional balance of the hemagglutinin and neuraminidase activities accompanies the emergence of the 2009 H1N1 influenza pandemic. J.Virol. 86, 9221–9232. [PubMed: 22718832]

Xu R, de Vries RP, Zhu X, Nycholat CM, McBride R, Yu W, Paulson JC, and Wilson IA (2013). Preferential recognition of avian-like receptors in human influenza A H7N9 viruses. Science 342, 1230–1235. [PubMed: 24311689]

Zamora CY, d'Alarcao M, and Kumar K (2013). Fluorogenic sialic acid glycosides for quantification of sialidase activity upon unnatural substrates. Bio-org. Med. Chem. Lett 23, 3406–3410.

Zhu X, McBride R, Nycholat CM, Yu W, Paulson JC, and Wilson IA (2012). Influenza virus neuraminidases with reduced enzymatic activity that avidly bind sialic acid receptors. J. Virol. 86, 13371–13383. [PubMed: 23015718]

Zou Y, Wu Z, Chen L, Liu X, Gu G, Xue M, Wang PG, and Chen M (2012). An efficient approach for large-scale production of sialyglycopeptides from egg yolks. J. Carb. Chem. 31, 436–446.

Highlights

- Influenza A virus hemagglutinins exclusively bind either NeuAc or NeuGc sialic acids
- Structural studies reveal this specificity at the atomic level
- Influenza A virus neuraminidases are able to cleave NeuGc
- NeuGc specificity represents a species barrier

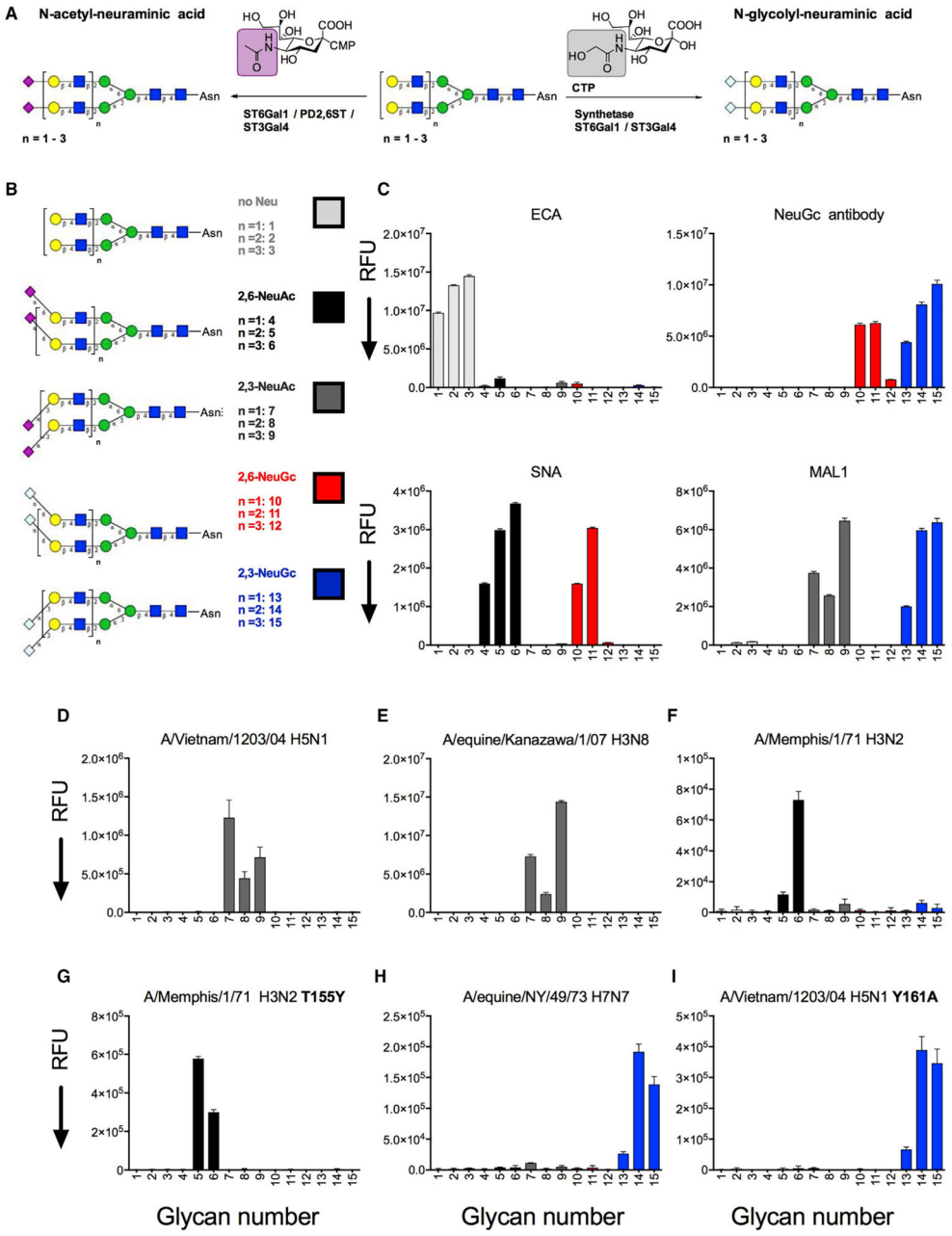

Figure 1. A Glycan Microarray Containing NeuGc Glycans

(A) Synthesis of the compound library. (Left) Previously described by Nycholat et al. (2012). (Right) Synthesized in this project. The difference between N-acetyl (NeuAc) and N-glycolyl (NeuGc) is highlighted in the colored boxes. See also Data S1.

(B) Overview of the synthetic glycans printed on the microarray (n = 6). See also Figure S1.

(C) Verification of the microarray with control lectins: ECA, α-N-glycolyl IgY, SNA, and MAL1. A representative of three independent assays is shown. See also Table S1, S2, and S3.

(D–I) Evaluation of receptor specificity of HA proteins toward human and avian-type receptors containing either N-acetyl or N-glycolyl. The glycan microarray was used to

determine the receptor specificities of several wild-type and mutant HAs: (D) A/Vietnam/1203/04 H5N1, (E) A/equine/Kanazawa/1/07 H3N8, (F) A/Memphis1/71 H3N2, (G) A/Memphis1/71 H3N2 T155Y, (H) A/equine/NY/49/73, H7N7, and (I) A/Vietnam/1203/04 Y161A H5N1.

The mean signal and standard deviation were calculated for each glycan printed in replicates of 6. The data are representative of three independent assays using independently made protein preparations. α2,6-linked N-acetyl is shown in black bars (glycans 4–6), α2,3-linked N-acetyl in gray (glycans 7–9), α2,6-linked N-glycolyl in red (glycans 10–12), and α2,3-linked N-glycolyl in blue (glycans 13–15). Glycans 1 −3 are non-sialylated controls and are shown in light gray bars.

See also Table S2 and S3 and Figure S2.

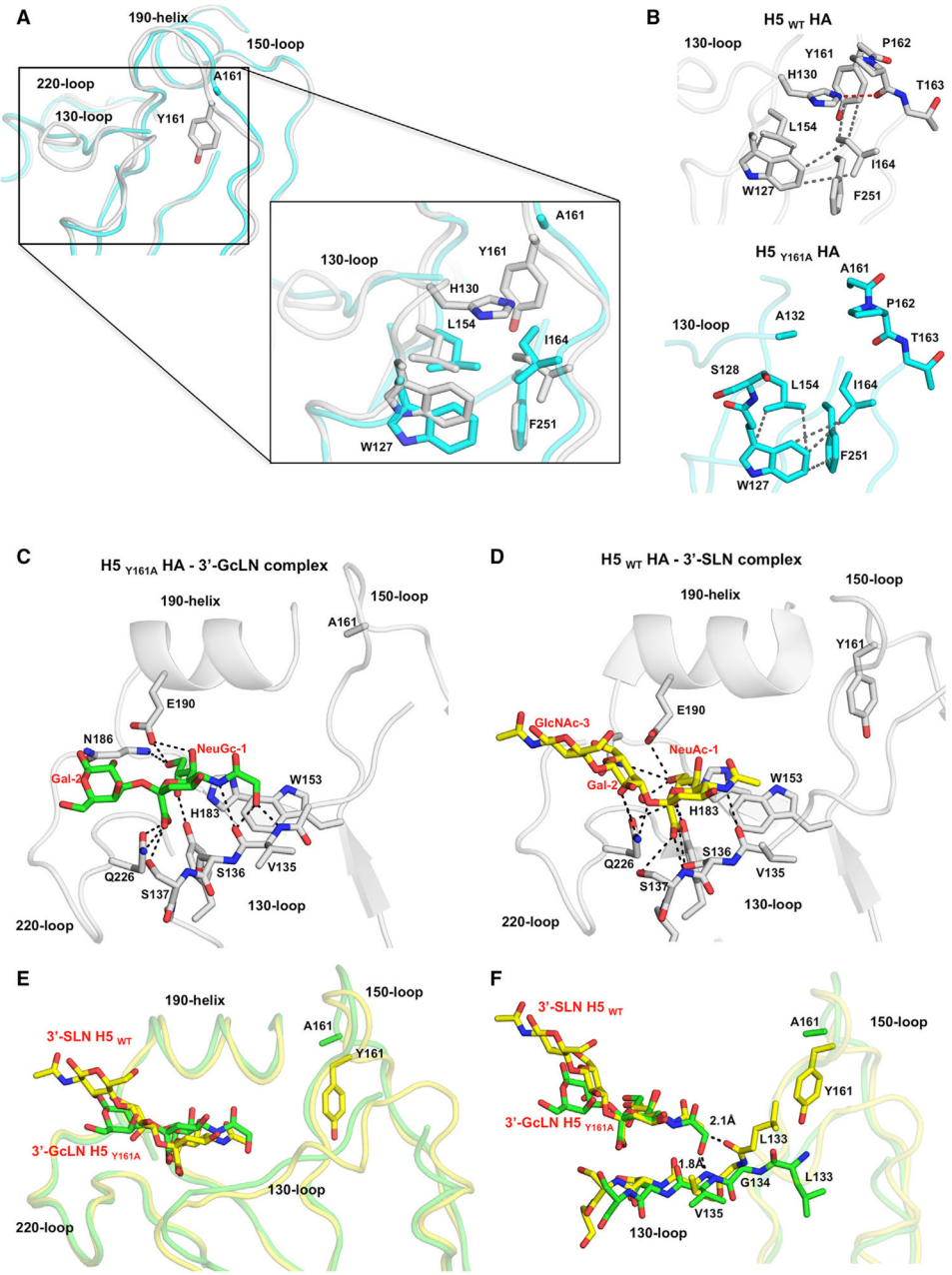

Figure 2. Crystal Structures of the H5 Y161A Mutant in Apo Form and in Complex with 3′-GcLN Receptor Analog

(A) Superposition of the structures of H5 Y161A HA (in cyan) and wild-type H5 HA (PDB: 2FK0, gray), indicating the conformational changes due to the Y161A mutation. The conserved secondary elements of the HA RBS are labeled and shown in tube representation. (B) The hydrophobic core that forms by W127, L154, I164, Y161, and F251 in the structures of H5 wild-type (right) and H5 Y161A mutant (left) HAs. The hydrophobic interactions are shown in gray dashes and the hydrogen bond between H130 and P162 in red dashes.

(C and D) Hydrogen bond interactions between the RBS of the H5 Y161A mutant and receptor analog 3′-GcLN (C) and the RBS of H5 wild-type (WT) with receptor analog 3′-SLN (D). The conserved secondary elements of the HA RBS are labeled and shown in tube representation, and receptor analogs and RBS residues are labeled and shown in sticks.
(E) Superposition of the crystal structures of H5 Y161A HA in complex with the 3′-N-glycolyl analog (green) with H5 HA in complex with avian receptor analog 3′-SLN (yellow) indicating the displacement of N-glycolyl-1 away from the base of the RBS. The superposition was performed on the RBS subdomain (residues 117–265 of HA1).
(F) Superposition of N-glycolyl-1 from H5 Y161A structure, and N-acetyl-1 from H5 wild-type HA structure, suggests potential structural clashes between the N-glycolyl group of N-glycolyl-1 to the main chains of L133 and V135 from the 130-loop. The distances between the N-glycolyl group to L133 and V135 of H5 wild-type are indicated.
See also Table S4 and Figure S3.

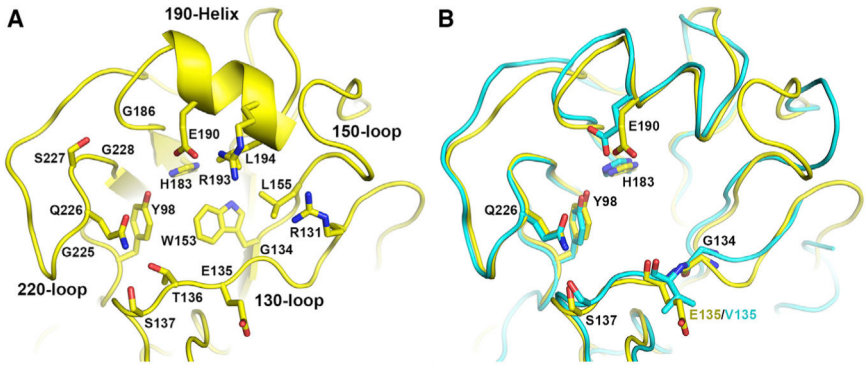

Figure 3. Crystal Structure of Equine H7 HA in Apo Form

(A) The RBS of the equine H7 HA with binding site residue side chains shown in stick representation.

(B) Superposition of the RBS structures of equine H7 HA (in yellow) and apo H5 Y161A HA (cyan) with some key binding residues shown in stick representation.

See also Table S4.

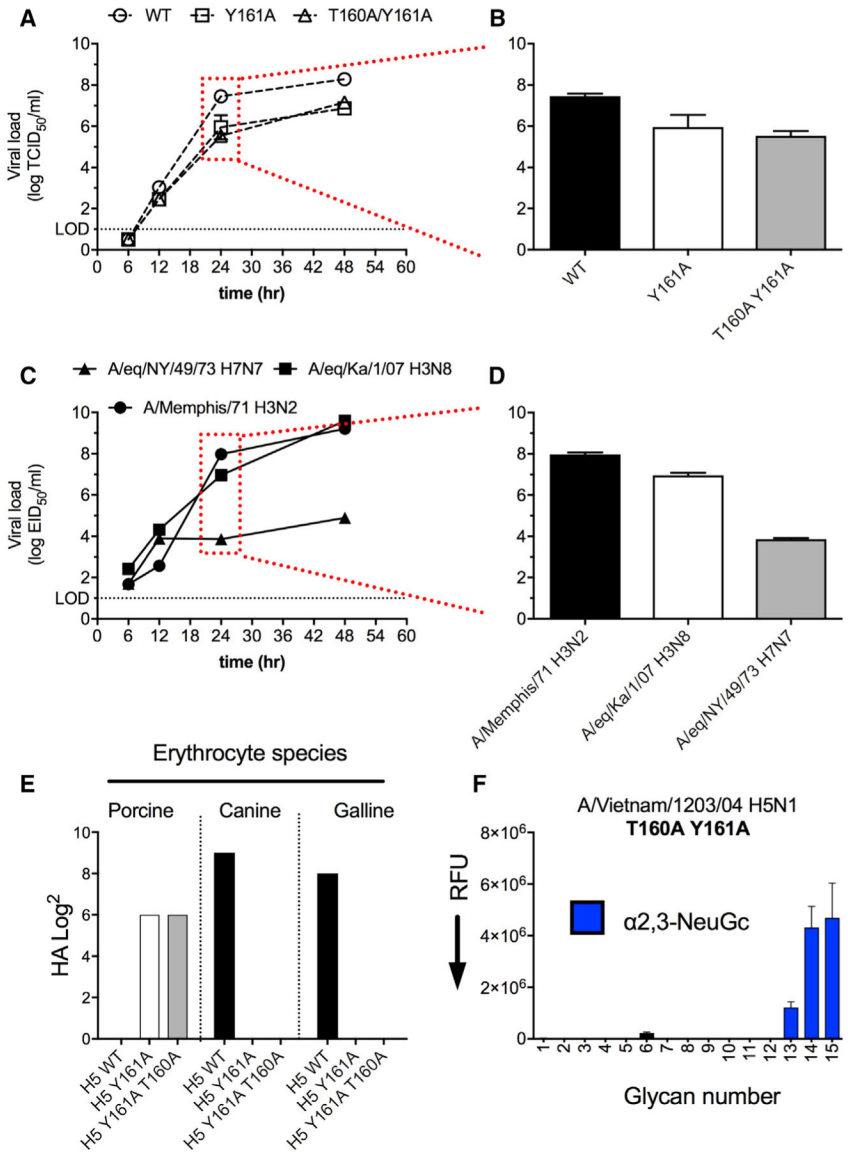

Figure 4. Infectivity of Different N-acetyl- and N-glycolyl-Specific Viruses

(A and B) Growth properties of the recombinant H5 viruses on MDCK cells at different time points (A) and bar graphs at 24 h post infection (B); a representative of three independent assays is shown.

(C and D) Growth properties of the H3 and H7 viruses on MDCK cells at different time points (A) and bar graphs at 24 h post infection (B); a representative of three independent assays is shown.

(E) Hemagglutination assay using porcine, canine, and galline erythrocytes with A/Vietnam/1203/04 wild-type, Y161A, and T160A Y161A double mutant as recombinant proteins. The data are representative of three independent assays performed in triplicate, using independently made protein preparations.

(F) Glycan microarray analysis of the T160A Y161A mutant that maintains a strict specificity for α2-3-linked N-glycolyl. The mean signal and standard deviation were

calculated for each glycan printed in replicates of 6. The data are representative of three independent assays using independently made protein preparations.
See also Table S3 and Figure S4.

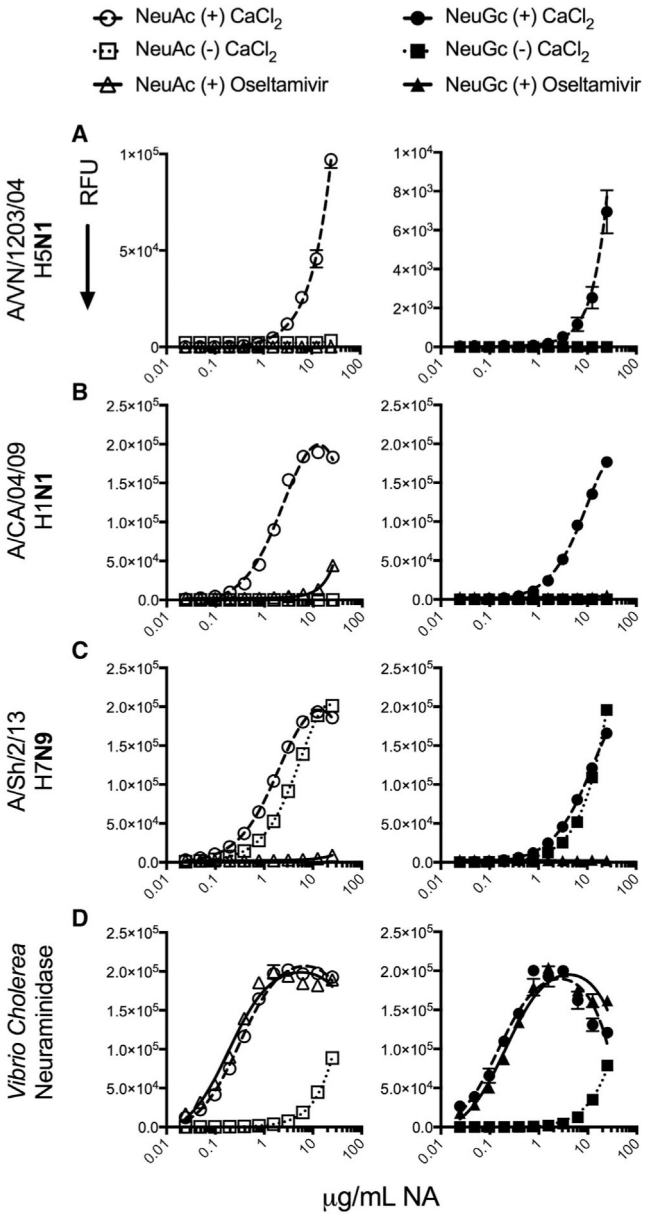

Figure 5. Neuraminidase Activity and Specificity toward N-acetyl and N-glycolyl

NA activity was measured by a solution-based assay using fluorescent substrate 4-MU-NANA and NGNA (see also Scheme S1). Tested neuraminidases are in the presence and absence of $CaCl_2$ and oseltamivir carboxylate, and representative of three independent assays all done in triplicate, with independent protein preparations: (A) A/Vietnam/1203/04 H5N1, (B) A/CA/04/09 H1N1, (C) A/Sh/2/13 H7N9, and (D) Vibrio cholerae NA.

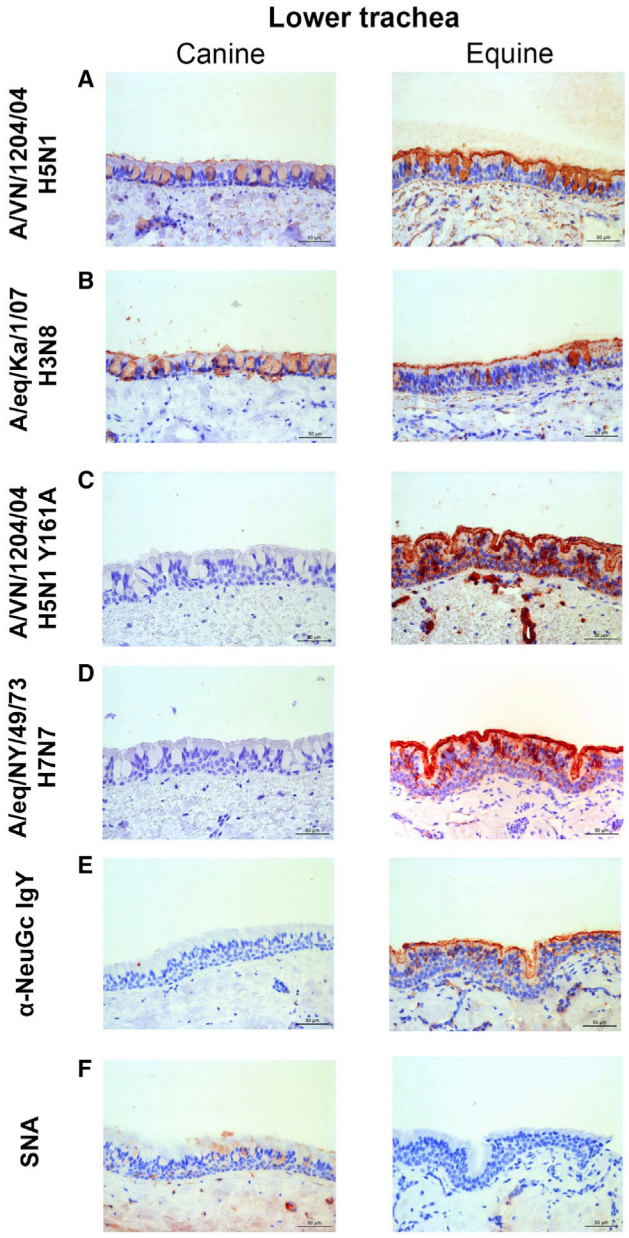

Figure 6. Tissue Binding Specificity of HA to Canine and Equine Tracheal Epithelium

Tissue binding is visualized by AEC staining and representative of three independent assays with independent protein preparations: (A) A/Vietnam/1203/04 H5N1, (B) A/equine/Kanazawa/1/07 H3N8, (C) A/Vietnam/1203/04 H5N1 Y161A, (D) A/equine/NY/49/73 H7N7, (E) α-N-glycolyl IgY, and (F) SNA.

KEY RESOURCES TABLE

REAGENT or RESOURCE	SOURCE	IDENTIFIER
Antibodies		
Mouse anti-StrepTag	IBA	Cat #2-1509-001
Goat anti-Mouse IgG-647	Thermo	Cat # A28181; RRID: AB_2536165
Anti-NeuGc IgY	Biolegend	Cat # 146903; RRID: AB_2562884
Bacterial and Virus Strains		
A/Vietnam/1203/04/H5N1	This paper	NCBI:txid284218
Biological Samples		
β3GnTII	Expressed according to (Prudden et al., 2017) and (Moremen et al., 2018)	N/A
GalT	Roche Diagnostics	Cat #07215118103
PD2,6ST	Chemily LLC	Cat # EN01001
ST6Gal1	Expressed according to (Moremen et al., 2018)	N/A
ST3Gal4	Expressed according to (Moremen et al., 2018)	N/A
CMP-Sialic acid synthetase	Expressed according to (Karwaski et al., 2002)	N/A
Calf intestine alkaline phosphatase	Sigma Aldrich	Cat # P4978
Erythrina cristagalli agglutinin	Vector Labs	Cat # B-1145
Sambuca nigra agglutinin	Vector Labs	Cat # B-1305
Maackia amurensis	Vector Labs	Cat # B-1315
Chemicals, Peptides, and Recombinant Proteins		
UDP-Gal,	Roche	Cat #07703562103
UDP-GlcNAc	Roche	Cat # 11787900103
CMP-Sialic	Roche	Cat # 05974003103
CTP	Chemily	CAS 3605-68-0
4-MU-NANA	Sigma	Cat # M8639-5MG
Streptavidin-AlexaFluor635	Thermo	Cat # S32634
4-MU-NGNA	This paper	N/A
3-amino-9-ethyl-carbazole	Sigma	Cat # A6926
Deposited Data		
H5N1 Y161A Apo form	This paper	PDB: 6E7G
H5N1 Y161A in complex with 3′-GcLN	This paper	PDB: 6E7H
A/equine/NY/49/73 HA	This paper	PDB: 6N5A
A/equine/NY/49/73 HA cDNA	NCBI	LC414434
Experimental Models: Cell Lines		
HEK293S GnTI(−)	ATCC	CRL-3022
MDCK	ATCC	CRL-2936
Oligonucleotides		
available upon request	This paper	N/A
Recombinant DNA		
A/Vietnam/1203/04/H5N1	(de Vries et al., 2014), NCBI	284218
A/Indonesia/05/05/H5N1	(de Vries et al., 2014), NCBI	EF541394

REAGENT or RESOURCE	SOURCE	IDENTIFIER
A/Memphis/1/71/H3N2	NCBI	AB298687
A/equine/Kanazawa/1/07H3N8	(Motoshima et al., 2011), NCBI	AB369862
A/CA/04/09/pdmH1N1	(de Vries et al., 2011), NCBI	FJ966082
A/swine/Ohio/891/01/H1N2	(de Vries et al., 2011), NCBI	AF455675
A/KY/UR-06-0258/07/H1N1	(de Vries et al., 2011), NCBI	CY028163
A/Puerto Rico/8/34/190E/H1N1	(Nemanichvili et al., 2019), NCBI	NP_040980.1
A/canine/TX/01/04	F. Krammer Mt Sinai, NCBI	ABA39850.1
A/duck/Hokkaido/111/09/H1N5	https://virusdb.czc.hokudai.ac.jp/, NCBI	AB560963
A/duck/Hokkaido/95/01/H2N2	https://virusdb.czc.hokudai.ac.jp/, NCBI	AB276115
A/duck/Hokkaido/138/07/H4N6	https://virusdb.czc.hokudai.ac.jp/, NCBI	AB450439
A/equine/NY/49/73/H7N7	https://virusdb.czc.hokudai.ac.jp/, NCBI	LC414434
Other		
NHS-ester activated glass slides	N/A	(NEXTERION ® Slide H, Schott Inc.)